Desalination and Water Treatment
www.deswater.com
doi: 10.5004/dwt.2020.26039

196 (2020) 315–328
August

Fast adsorption–desorption of Eriochrome Black T using superparamagnetic NiZn ferrite nanoparticles

Lotfi Ben Tahar[a,b,c,*], Mohamed Habib Oueslati[a,d]

[a]*College of Science of Arar, Northern Border University, P.O. Box: 1231, Arar 91431, Saudi Arabia, Tel. +966 5 00 88 65 85/ +216 98 902 376; emails: bentaharlotfi@gmail.com (L.B. Tahar), ouesmed74@gmail.com (M.H. Oueslati)*
[b]*Laboratoire des Composés Hétéro-Organiques et des Matériaux Nanostructurés (LR18 ES11), Faculté des Sciences de Bizerte, Université de Carthage, 7021, Zarzouna, Tunisia*
[c]*Faculté des Sciences de Tunis, Université de Tunis El Manar, Campus Universitaire, 2092, Tunisia*
[d]*Department of Chemistry, Preparatory Institute for Scientific and Technical Studies, Carthage University, P.O. Box: 51, La Marsa 2070, Tunisia*

Received 23 November 2019; Accepted 27 April 2020

ABSTRACT

This work describes the preparation, the characterization, and the magnetic properties of a series of three mixed NiZn ferrite nanoparticles and the study of their efficiency for the adsorption–desorption of Eriochrome black T (EBT) dye. The nanoferrites were produced by the coprecipitation method. The produced powders were pure phases with a cubic spinel-type ferrite structure. They consisted of almost spherical nanoparticles with an average size ranging from ~13.5 to 16 nm. The smallest size was observed with the ferrite (abbreviated to as NiZn1) which exhibited the largest Zn content. Magnetic study revealed a superparamagnetic behavior at room temperature with a reasonable saturation magnetization and a relatively high Curie temperature. Adsorption, desorption, and regeneration study of EBT onto the nanoparticles was achieved by varying the nanoparticle nature, the pH, the nanoparticle dosage, the contact time, and the dye concentration. Regarding the effect of the nanoparticle nature on the removal of EBT, the smallest nanoparticles (NiZn1) were noticeably more performant. For these nanoparticles, the removal efficiency was found to increase with the decrease of pH. At pH 2.0, the adsorption of EBT onto NiZn1 nanoparticles was fast and the uptake capacity was found to decrease with the adsorbent dosage. Three kinetic models were tested. The best fitting to the kinetic data ($R^2 > 0.986$) was with the pseudo-second-order model. The adsorption capacity, q_e, of NiZn1 was found to increase with the increase of the adsorbate concentration. For instance, for the EBT dosage of 4.0 g L^{-1}, q_e, was found to range from 12.5 for 50 to 34.4 mg g^{-1} for 250 mg g^{-1}. The selected NiZn1 nanoadsorbent was tested in six adsorption–desorption-reuse cycles without significant loss in sorption/desorption performance.

Keywords: Mixed ferrite; Nanoparticles; Superparamagnetism; Curie temperature; Eriochrome Black T; Dye removal; Adsorption; Kinetics; Regeneration

1. Introduction

The spinel-type ferrites is a class of wide range of ferric oxides (including the fully oxidized maghemite, γ-Fe_2O_3) with the general chemical formula $M^{2+}Fe_2^{3+}O_4$ (M = Fe, Ni, Cu, Zn, Co, (Co,Zn), (Ni,Zn), etc.). They exhibit an almost close packing cubic arrangement of oxide ions that form tetrahedral (A) and octahedra (B) sites, where the metal ions reside [1]. In recent years, nanosized spinel-type ferrite-based materials have gained great attention owing to their unique and tuneable physicochemical features,

* Corresponding author.

in particular, the magnetic and the electrical properties. These properties are strongly dependent on several intrinsic and extrinsic parameters such as the cation's occupancy over A and B sites (which in turn is strongly dependent on the elaboration history), the surface chemistry, the microstructure, the interparticle magnetic interaction, etc. [1–3]. Spinel-type nanoferrites find wide applications in various fields, such as biomedicine, energy storage, water treatment, electronics, optics, electrochemistry, catalysis, etc. [4–9]. The rapid development of industrial activities increased the amount of wastewater discharged into water bodies. The discharged wastewater contains different organic and inorganic pollutants that are highly toxic and harmful to the environment. An important fraction of the chemical species resist degradation and are environmentally persistent which required developing new approaches to tackle this problem [10]. In addition, many molecules (synthetic dyes, insecticides, pesticides, etc.) are highly colorized and some of them may also cause allergies, dermatitis, skin irritation, or cancer to humans and might lead to genetic mutations [11]. Besides, dyes can also seriously affect aquatic life by affecting negatively the growth of marine plants. The most used wastewaters processing treatments routes (the chemical routes, the coagulation, and flocculation, the biological treatment) present several drawbacks like the high operational cost, the lack of selectivity, the release of harmful by-products, the difficulty of recycling the treatment reagents and the incomplete removal of the pollutant. Adsorption technique using magnetic-based nanomaterials (especially the spinel-type ferrites) has demonstrated great potential to overcome most of the above-mentioned issues [12–15]. Recently, spinel-type ferrites have been extensively used as magnetic adsorbents to remove both cationic and anionic azo dye molecules (organic compounds containing the linkage C–N=N–C) from aqueous solutions. Their superiority owes to their high specific surface area, high dispersion ability, reasonable magnetic performance, biocompatibility, reusability, and cost-effectiveness. Eriochrome Black T (EBT) was used as a model adsorbate for the adsorptive removal of synthetic azo anionic dyes from wastewaters using various adsorbents [11,16–21]. While, to the best of our knowledge, only few studies have been dedicated to the use of magnetically guided and reusable ultrafine particles for the EBT uptake [19,22,23]. For instance, Moeinpour et al. reported the adsorption studies under various parameters, such as pH, contact time, initial dye concentration and adsorbent dosage using 50 nm nanosized $NiFe_2O_4$ ferrite produced by the coprecipitation method. The maximum adsorption occurred at the pH value of 6.0 with an adsorption capacity of 47.0 mg g^{-1} of adsorbent [19]. Attallah et al. [22] reported the chemical synthesis of magnetite nanoparticles modified with pectin shell and silica/pectin double shell, and then tested them for single dye and dye mixture adsorption from water samples. Saha et al. [23] studied the adsorption of different dyes (including EBT) on the magnetite (Fe_3O_4) having an average size of 20–40 nm. The ferrite has been synthesized by coprecipitation of divalent and trivalent iron salts using triethylamine as base and the sodium dodecyl sulfate as a stabilizing agent. For EBT, maximum adsorption capacity of ~89 mg g^{-1} of adsorbent was found at pH ~4.0–5.0, then it decreases with the increase of pH beyond the pH values [23]. The relatively high adsorption capacity of EBT as compared to the other dyes was ascribed to the existence of additional hydroxyl (–OH) groups in the molecular structure of EBT. For EBT dye, a maximum uptake capacity of ~65 and 72 mg g^{-1} of adsorbent was reported for magnetite/silica/pectin and magnetite/pectin, respectively. The highest adsorption efficiency was observed to occur in high acidic medium (pH = 2). It is expected that the Fe^{2+}-based iron oxide nanoparticles such as Fe_3O_4 and its derivatives are not chemically stable, in particular, in acidic aqueous media which seriously limits their long-term reusability in any adsorption process [24]. Further, for efficient and fast removal of the contaminant-loaded adsorbent by an external magnetic field, producing magnetic nanoparticles with reasonable magnetization in crucial. This could be fulfilled by the synthesis of mixed spinel-ferrites with adjusted substitution of the paramagnetic metal cations with nonmagnetic metal cations like Zn^{2+}, Cd^{2+}, etc. In the context, a series of superparamagnetic NiZn mixed ferrites was produced by the coprecipitation method and then characterized by various techniques such as X-ray diffraction (XRD), energy dispersive X-ray (EDX), Infrared (IR), UV-visible, transmission electron microscopy (TEM), and squid magnetometry. Then, we investigated the adsorptive removal by the produced nanomaterials of EBT as a model of azo dyes from synthetic wastewaters by studying the effect of selected physicochemical parameters like the nanoparticle nature, the pH, the adsorbent dosage, and the contact time.

2. Experimental

2.1. Nanoparticles synthesis

Three Nickel–Zinc mixed ferrite nanoparticles with different degrees of zinc substitution and a nominal molar ratio ([Ni] + [Zn])/[Fe] = 0.5, were produced by the chemical co-precipitation route, introducing some modifications to the method described by Zins et al. [25]. For our preparations, the chosen degrees of zinc substitution defined by the nominal molar ratio R_0 = [Zn]/([Ni] + [Zn]) were 0.5, 0.33, and 0.25. The corresponding nominal chemical formula are $Ni_{0.5}Zn_{0.5}Fe_2O_4$, $Ni_{0.66}Zn_{0.33}Fe_2O_4$, and $Ni_{0.75}Zn_{0.25}Fe_2O_4$, respectively. For the sake simplicity in notation, the preparations, and the resulting mixed ferrites are hereafter denoted as NiZn1, NiZn2, and NiZn3, for the ratio 0.5, 0.33, and 0.25, respectively. In a typical procedure (for the preparation of NiZn1), acidified freshly solutions, of $FeCl_3$ (160 mL, 1.0 M; Techno Pharmchem, Haryana, India, 98%), $NiCl_2{\cdot}6H_2O$ (40 mL, 1.0 M; InterChem, UK, 97%) and $ZnCl_2$ (40 mL, 1.0 M; Loba Chemie, India, 98%) were prepared and mixed vigorously in a 2,000 mL capacity conical flask. To the reaction, the medium was then quickly poured 1.0 L of 1.0 M NaOH solution. A dark brownish precipitate formed immediately. The reaction medium was subjected to additional simultaneous vigorous magnetic stirring and heating for 90 min. The obtained precipitate was allowed to cool and to settle overnight. The supernatant was then discarded from the precipitate with the aid of a NdFeB magnet. The precipitate was then washed several times with an excess of ultrapure water until an almost neutral pH is reached. The obtained wet precipitate was vigorously

stirred in 100 mL of 2 M nitric acid solution for about 20 min resulting in a very stable black colloid. The cationic magnetic colloid obtained directly after this treatment was not chemically stable with time. A gradual dissolution of particles and gelation of solution took place. To prevent this dissolution, to the previously obtained acidic suspension was added an acidified aqueous solution of metal nitrates (98%) purchased from Techno Pharmchem, Haryana, India [$Fe(NO_3)_3$: 140 mL, 0.5 M; $Ni(NO_3)_2$: 70-z' mL, 0.5 M; $Zn(NO_3)_2$: z' mL, 0.5 M (with $z' = 70\ R_0$)]. The obtained solution was heated to boiling under vigorous stirring for about 40 min. It is noticed that on boiling, the previously observed dark brownish color re-appeared. The brownish precipitate was allowed to cool and settle overnight. The supernatant was isolated from the precipitate with the aid of a NdFeB magnet. Subsequently, an excess of ultrapure water was added, and the precipitate was washed in order to remove the excess of dissolved salts. Note, while washing, a rapid decantation of the magnetic precipitate can be performed by adding an excess of 1.0 M NaOH solution. The resulting precipitate was washed with excess of ultrapure water under magnetic decantation. Once a neutral pH of the supernatant was reached, the precipitate is dried at 80°C in a hot air oven for further use.

It is worthening that in the washing/decantation step, a pale red to brownish color supernatant was observed for all the preparations. This is believed to be due to the presence of fraction of ultrafine particles that couldn't be easily decanted magnetically, thus indicating a polydispersity in the produced nanoparticles.

2.2. Batch adsorption experiments

The effect of various parameters including the nanoparticle nature, the pH, the nanoparticle dose, the contact time, and the EBT initial concentration, on the adsorption efficiency, the adsorption kinetics, the desorption, and the regeneration capacity of the produced NiZn ferrites, was studied at room temperature in a batch mode. For each adsorption experiment, a certain volume (in mL) of dye solution of known initial concentration was added to a certain amount of the adsorbent accurately weighted in a dry clean screw capped glass test tube. The agitation was carried out using intermittent ultrasonication/vortexing. After a certain time of contact, the nanoadsorbent was quickly (within seconds) separated from the mixture using a permanent strong neodymium iron boron magnet. For the determination of the residual amount of EBT in the collected supernatant, a calibration curve was plotted using a series of standard aqueous solutions (5–200 mg L^{-1}) of analytical grade EBT (Sigma-Aldrich, ≥99%, St. Louis, USA) dissolved in freshly prepared acidic or alkaline ultrapure water. The pH of EBT solutions (prior to the addition of the adsorbent) was adjusted to the desired value using 0.1 HCl and/or 0.1 NaOH solutions and the pH measurement was done using a pre-calibrated (pH 4.0 and 7.0) benchtop pH meter (Hach, SensION, England, UK). The UV-visible spectra were recorded in the 250–700 nm range against an aqueous solution of adjusted pH as blank, using a UV-visible double-beam spectrophotometer (Jasco V-670, England, UK) equipped with 1 cm wide quartz cells. The maximum absorbance at the wavelength, λ_{max} = 531 nm, was considered for the calculation of EBT concentration by extrapolation from the calibration curve.

The removal efficiency of EBT by the produced nanoparticles can be assessed by the percentage of EBT removal and the amount of dye adsorbed per unit mass (q) using the following equations:

$$\text{Removal}\,\% = \frac{C_0 - C_t}{C_0} \times 100 \tag{1}$$

$$q_t = \frac{C_0 - C_t}{m_{\text{adsorbent}}} \times V \tag{2}$$

where C_0 and C_t (in mg L^{-1}) are the initial concentration (at $t = 0$) and the concentration after t minutes of contact of the adsorbate species with the adsorbent, respectively; q_t is the adsorption capacity (in mg g^{-1}). It represents the amount (in mg) of adsorbate species removed by the adsorbent (in g) after t minutes of contact. V is the volume (in L) of the adsorbate solution used. $m_{\text{adsorbent}}$ is the mass (in g) of the adsorbent used.

2.3. Point of zero charge of the as-produced nanoferrites

The point of zero charge (pHpzc) of the as-produced nanoferrites was measured using 0.01 M NaCl solutions adjusted to different pH values (pH_i) in the range 2–12 by adding either a 0.1 N HCl or a 0.1 N NaOH solution. Thirty milligrams of each ferrite sample were contacted with 10 mL of each the abovementioned solutions and shacked for about 24 h. The preparation was then magnetically decanted, and the pH (pH_f) of the supernatant measured. The pHpzc (at $\Delta pH = 0$) value was determined from a plot of ($pH_f - pH_i$) vs. pH_i.

2.4. Characterization techniques

XRD data were collected at room temperature at a 2θ step scan of 0.05 on a Bruker D8 Advance X-ray diffractometer (Massachusetts, USA) operating at a voltage 40 KV and an electric current 40 mA and equipped with $Cu_{K\alpha}$ radiation (λ_{Cu} = 1.54056 Å). The XRD powder pattern indexing, the unit cell constant calculation and refinement, and the crystallite size were carried out using X'Pert HighScore Plus package [26]. From the line broadening of the most intense XRD diffraction peak (hkl: 311) and considering a Lorentzian profile function for the peaks refinement, the average crystallite size (L_{XRD}) of the powders contents was calculated using the Scherrer formula [27]:

$$B(2\theta) = \frac{k \times \lambda}{L \times \cos(\theta)} \tag{3}$$

where L represents the crystallite size (in nanometers), k is the shape factor (0.89 for spherical particles), λ is the wavelength of the $Cu_{K\alpha}$ radiation, B is the full width at half maximum (FWHM) of the diffraction peak and θ denotes Bragg's angle of the most intense XRD diffraction peak (*hkl*: 311). Mid-infrared (IR) characterization was carried in the 4,000–400 cm^{-1} range at a resolution better than 4 cm^{-1} on

a Nicolet UR 200 FT-IR (Fourier transform infrared) apparatus (Thermo Scientific, Massachusetts, USA) using the KBr pelleting technique. Elemental chemical analysis was conducted with an EDX detector mounted on a FEI Quanta 450 scanning electron microscopy (SEM). The particle morphology was observed by a JEOL 2100F-LM microscope TEM (Tokyo, Japan) operating at 200 kV. Particle size distribution was derived considering at least 150 particles measured on randomly chosen TEM micrographs. Specimens were prepared by dispersing the powder in acetone and dropping the suspensions on copper grids coated with carbon support films. The magnetic measurements of the three ferrites under study were conducted on a quantum design PPMS VSM (Physical Property Measurement System – vibrating sample magnetometer). The hysteresis loops were measured with magnetic field cycling between +50 and –50 kOe at 300 K and the temperature-dependent magnetization was recorded in the temperature range 50–330 K under a fixed magnetic field of 20 kOe.

3. Results and discussion

3.1. Phase analysis

EDX and elemental mapping analysis carried out at randomly selected areas of sample revealed the expected metallic elements, for instance Fe, Ni, and Zn. Typical EDX spectra are shown in Fig. 1. Quantitative analysis inferred from EDX analysis permits the determination of the chemical formula of the as-produced three NiZn ferrites. They are $Ni_{0.44}Zn_{0.56}Fe_{2.0}O_4$, $Ni_{0.37}Zn_{0.44}Fe_{2.13}O_4$, and $Ni_{0.35}Zn_{0.35}Fe_{2.19}O_4$ for NiZn1, NiZn2, and NiZn3, respectively. As can be clearly noticed, the chemical formula departs slightly from the expected chemical formula, calculated based on the nominal molar ratios.

Fig. 2 shows the XRD patterns of prepared samples. All the XRD peaks can be indexed in the cubic spinel structure with no extra lines corresponding to any other phase, indicating that the prepared ferrites are single phase. From the zoom-view around the most intense peak (inset in Fig. 2), it is seen that the peaks positions of NiZn2 and NiZn3 are very close. While those of NiZn1 have relatively slightly lower 2θ values.

Fitted values of the unit cell parameters of the NiZn ferrites are gathered in Table 1. These values are comparable to those reported for other NiZn ferrites (for instance [28,29]). As expected, the cell parameter of NiZn2 and NiZn3 are very close. While that of NiZn1 is slightly larger in agreement with the chemical formula inferred from EDX analysis in which the last ferrite presents the larger Zn content. Indeed, on the basis on the ionic radii of the constituting metal cations, namely Ni^{2+}, Zn^{2+}, and Fe^{3+},

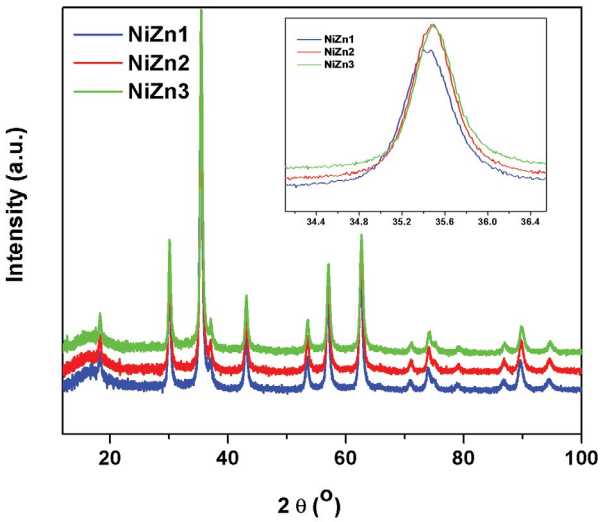

Fig. 2. XRD patterns of the as-prepared NiZn1, NiZn2, and NiZn3 powders. The inset is a zoom-view around the most intense peak (*hkl*: 311) showing the relative shift and the broadening of the XRD peaks.

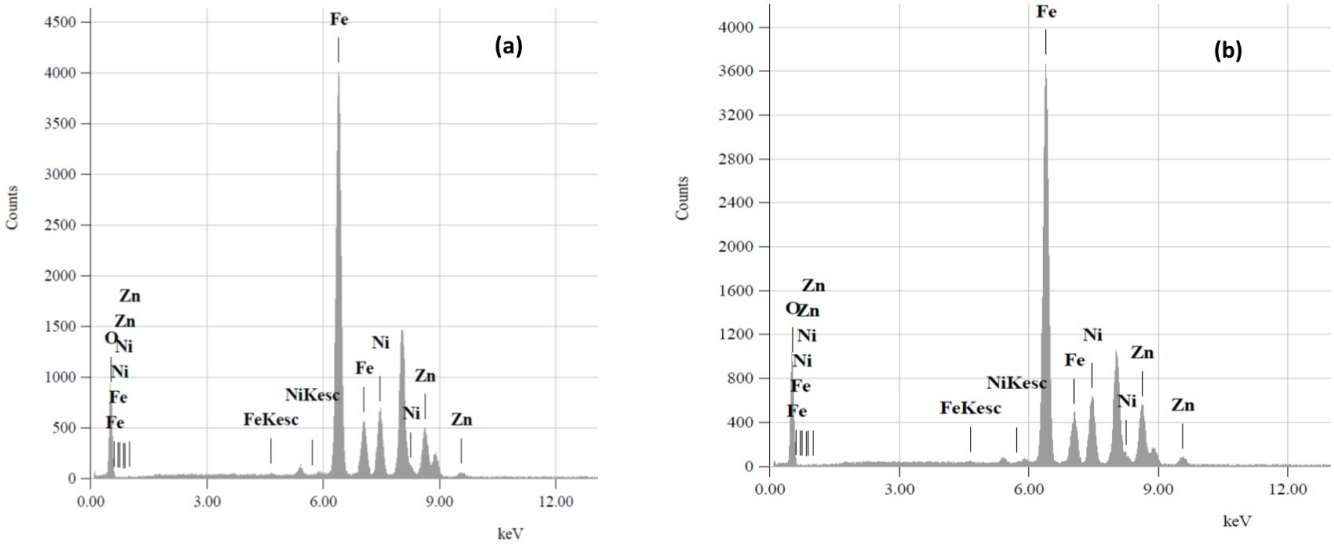

Fig. 1. EDX spectra of selected NiZn powders: (a) NiZn1 and (b) NiZn3.

the notably larger Zn content observed with EDX should result in the largest lattice parameter calculated for NiZn1.

Fig. 3 shows the Mid IR spectra of the produced nanoferrites recorded at room temperature.

Below 1,000 cm^{-1}, the IR spectra show two main absorption bands at around 590 and 430 cm^{-1}, which is a common feature of spinel-type ferrites [26]. The two bands are due to the intrinsic vibrations of tetrahedral and octahedral metal–oxygen complexes, respectively. The very intense broad band centred at around 3,430 cm^{-1} and the sharper one located at 1,640 cm^{-1} are, respectively, assigned to the stretching and the bending vibrations of hydroxyl groups. The OH groups are attributable to the adsorbed water molecules and very probably also to the hydroxyl groups coming from the alkaline medium (NaOH solution) in which the as-produced particles were decanted during their separation from their supernatant (section 2.1 (Nanoparticles synthesis)). The last suggestion is supported by the measurement of the point of zero charge (not shown) of the as-produced particles which is found to be slightly larger than 7.0. Finally, the broad and intense band located at around 1,075 cm^{-1} and the very sharp one centered at 1,385 cm^{-1} are ascribable to the vibrational modes in NO_3^- groups [25,30]. The NO_3^- species arise from the metal salt nitrates used in the final preparation step of the as-produced ferrites (section 2.1 "Nanoparticles synthesis").

3.2. Point of zero charge

The plot (pH_f – pH_i) vs. pH_i for the determination of the point of zero charge of the as-produced nanoferrites is depicted in Fig. 4.

The surface charge is positive for pH < pH_{PZC} and negative for pH > pH_{PZC}. In the case of our ferrites, the point of zero charge being located close to pH 7 (Table 1). These values fall in the range reported in the literature for iron oxides [31,32]. The NiZn ferrites can be considered as amphoteric solids, which can develop charges in the protonation reaction in acid medium (≡Fe–OH + H^+ ↔ ≡Fe–OH_2^+) and deprotonation reaction in basic medium (≡Fe–OH ↔ ≡Fe–O^- + H^+), where, ≡ denotes the surface of the nanoparticle. These surface reactions can be interpreted as the specific adsorption of H^+ and OH^- ions at the hydrated solid/water interface [31]. Besides, it was observed that destabilization of a colloidal dispersion of the as-produced particles occurred at pH values ranging from about 4 to 9; A macroscopic phase separation between the supernatant and the all the magnetic particles could be clearly observed.

3.3. Microstructural analysis

For all produced powders, the XRD peaks show a clear broadening, as the result of a reduced particle size and/or lattice strain. Estimation of the particle size, L_{XRD}, from the peak broadening gives a mean value of ~16, 18, and 19 nm for the ferrites NiZn1, NiZn2, and NiZn3, respectively (Table 1). Morphology of the as-prepared NiZn powders was observed with TEM. The results are presented in Fig. 5 and listed in Table 1.

As can be clearly seen from TEM images, the particles of NiZn ferrites show important irregularity in both the size and the shape with some agglomeration. They are composed of polygonal plate-shaped nanoparticles of six or higher sides. The average particle size (calculated by measuring the average of the largest and the smallest length of each particle) ranges from 13 nm for NiZn1 to 16 nm for NiZn3. It is noticed that all the produced nanoparticles could be considered as single crystals since the average particle diameter determined by TEM agrees well with the crystallite size inferred from XRD (Table 1).

3.4. Magnetic analysis

Magnetization, *M*, as a function of applied magnetic field, *H*, measured for all samples at 300 K is shown in Fig. 6.

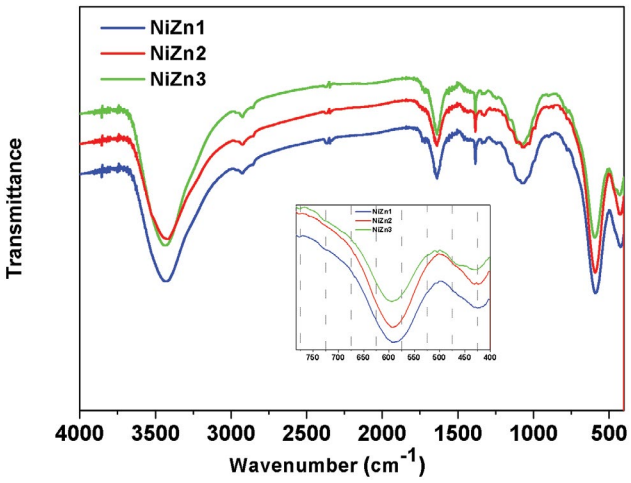

Fig. 3. IR spectra of the as-prepared NiZn1, NiZn2, and NiZn3 powders. The inset is a zoom-view around the band associated to the vibrational v_1 mode of Fe–O vibration.

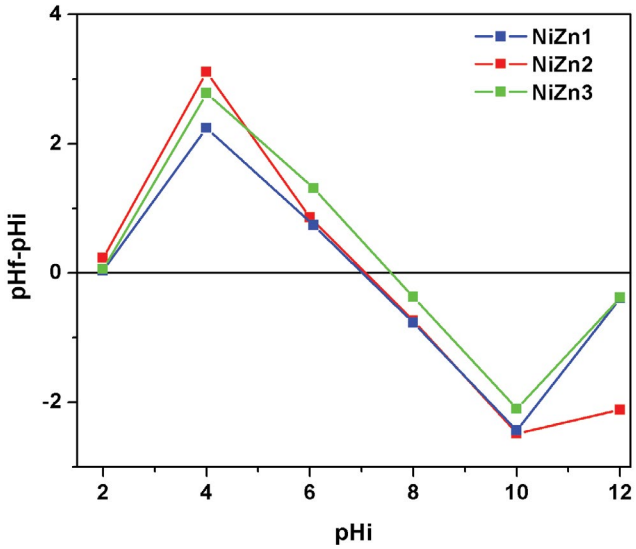

Fig. 4. Determination of the pH of the point of zero charge (pHpzc) of the as-produced NiZn1, NiZn2, and NiZn3 nanoparticles.

Table 1
pH of point of zero charge (pHpzc) and selected structural, microstructural, and magnetic characteristics of the as-produced NiZn ferrites

	a (Å)	L_{XRD} (nm)	$<D_{TEM}>$ (nm)	pHpzc	M_{sat} (300 K) [emu g^{-1}]	$M(0)$ [emu g^{-1}]	T_C (K)	$T_{1/2}$ (K)	β
NiZn1	8.397(1)	15.7	13.6 ± 2.2	7.02	55.5	81	621	372	1.3
NiZn2	8.3894(8)	18.1	15.4 ± 3.6	7.07	66.4	96	633	383	1.4
NiZn3	8.382(1)	18.5	16.1 ± 2.9	7.57	64.8	88	656	410	1.5

$M(0)$, T_C, and β, are the spontaneous magnetization at 0 K, the Curie temperature and the Bloch's exponent, respectively.

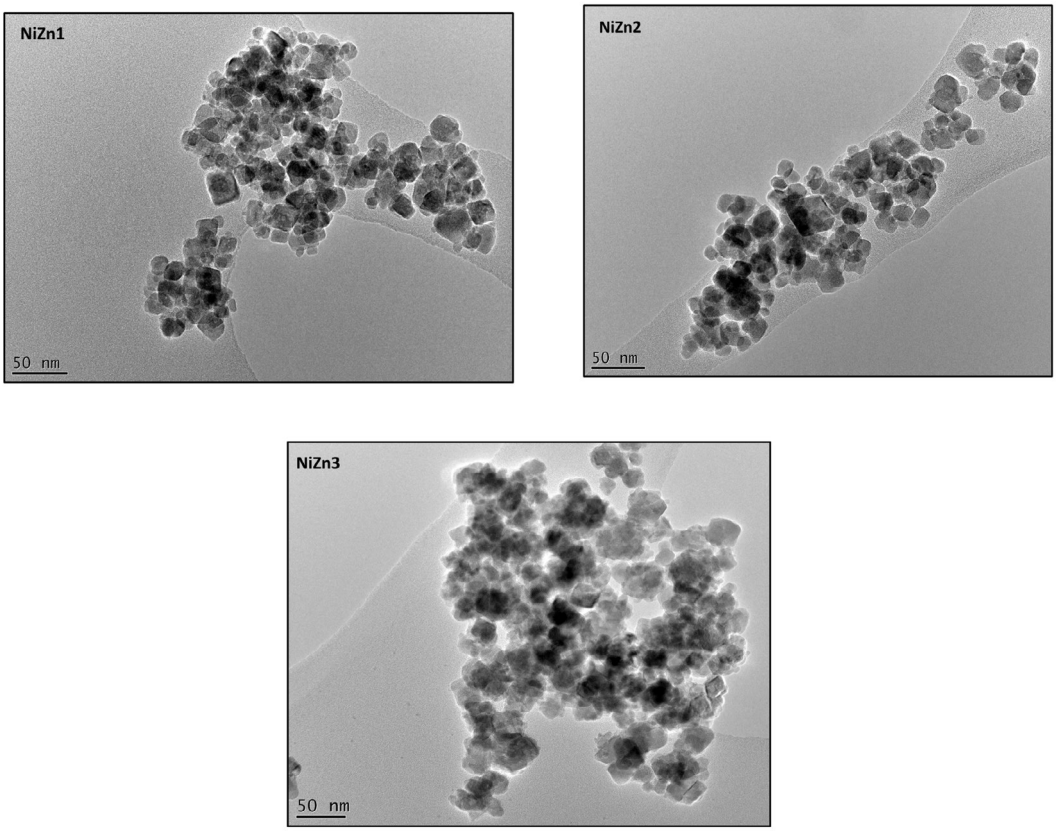

Fig. 5. TEM images of the as-prepared NiZn1, NiZn2, and NiZn3 powders.

At a first sight, there is neither remanence, nor coercivity, and then no hysteresis features, indicating a superparamagnetic behaviour of the produced nanoferrites at ambient temperature. Additionally, one can observe a similarity in the M vs. H curves of the NiZn2 and NiZn3 nanoparticles. In small ferromagnetic or ferrimagnetic single domain particles, superparamagnetism occurs above the so-called blocking temperature, T_B, because of weakly interacting and thermal fluctuations of the spins of the nanoparticles. The thermal effects allow flips of spins between the easy magnetization axes which lead to near zero-coercivity and increase in saturation magnetization [33]. In fact, a zoom view around H = 0 (Fig. 6), reveals the existence of a very weak hysteresis loop (non-zero coercivity (H_c) and non-zero remanence (M_{rem})). This is likely due to the existence of a small fraction of nanoparticles with a blocking temperature, T_B, above 300 K. The last result could be related to the polydispersity in size for the coprecipitation-made nanoparticles inducing a distribution in T_B [34]. The saturation magnetization, M_{sat}, values determined by extrapolating the magnetization vs. 1/H curve to 1/H = 0 are gathered in Table 1. They are of ~56, 66, and 65 emu g^{-1}, for NiZn1, NiZn2, and NiZn3, respectively. For our nanoparticles, M_{sat} values are large enough to be easily separated with a permanent magnet (inset in the upper-left of Fig. 6). At a given temperature, the magnetic features (M_{sat}, H_c, M_{rem}, etc.) of nanoparticles vary significantly with various intrinsic factors such as the core chemical composition, the average particle size, and the surface functionalization. In our case, the close magnetic features of NiZ2 and NiZn3 could be explained by the similarity of the chemical composition and the average particle size. While, the relatively reduced M_{sat} observed for NiZn1 could be related to the superposition of two factors: (i) a higher Zn^{2+} content (the chemical compositions); in the

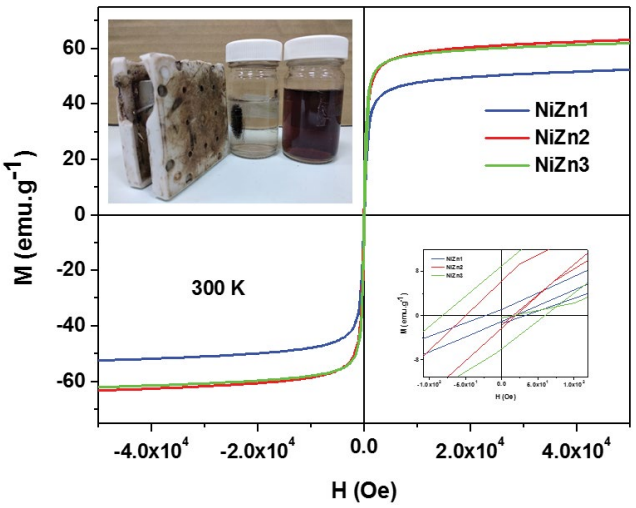

Fig. 6. Hysteresis loops measured at 300 K for the as-produced NiZn1, NiZn2, and NiZn3 nanoferrites. The inset in the down-right corner is a zoom-view around H ~ 0 showing the existence of small coercivity and remanence. The inset in the upper-left corner shows the magnetic separation of NiZn1 by an external magnetic field after adsorption of EBT dye onto the nanoparticles in comparison with an untreated EBT solution.

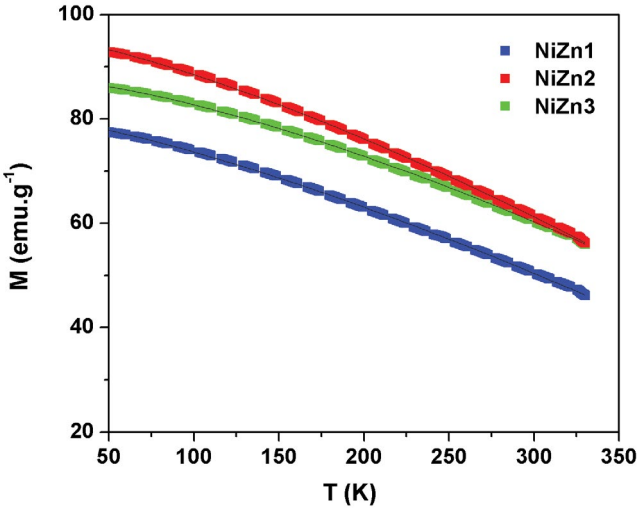

Fig. 7. Temperature-dependent magnetization decay, measured at 20 kOe for the as-produced NiZn1, NiZn2, and NiZn3 nanoferrites. The continued thin black lines are the best fit to the experimental data points to the modified Bloch's law.

mixed spinel-like structures, $(M^{2+})_{1-x}(Zn^{2+})_x(Fe^{3+})_2O_4$, where M^{2+} is a divalent paramagnetic ion, the magnetic dilution beyond a threshold Zn^{2+} content, induces a decrease in the magnetic interaction between the individual magnetic moments located in the tetrahedral (A) and the octahedral (B) spinel sites, resulting in a departure from the Néel's collinear model and therefore a decrease in M_{sat} [1]. (ii) a reduced particle size (Table 1); the lower value can be considered as a consequence of the finite size of the crystals which leads to a non-collinearity of magnetic moments near the surface. This is due to broken exchange bonds at the external layer of the particles resulting in a magnetically dead surface layer [35].

Temperature-dependent magnetization decay, measured at 20 kOe for the as-produced NiZn1, NiZn2, and NiZn3 nanoferrites is shown in Fig. 7.

As expected, the magnetization increases with decrease in temperature of the sample. Below, the Curie temperature the data points measured for the produced nanoferrites are well fitted ($R^2 > 0.999$) with the modified Bloch's law function [34].

$$M(T) = M(0) \times \left[1 - \left(\frac{T}{T_C}\right)^{\beta}\right] \quad (4)$$

Where $(1/T_C)^{\beta}$ is called the Bloch's constant (B) that depends upon the structure of the material. $M(0)$ is the spontaneous magnetization at 0 K and T_C is the temperature at which the saturation magnetization is zero. $M(T)$ is the temperature-dependent magnetization and β is the Bloch's exponent. The modified Bloch's law parameters are depicted in Table 1. In the spinel-type structures, the magnetic features depend on temperature and in a complex interdependent manner, on three intrinsic parameters including the nature of cations, their oxidation state, and their distribution over the spinel sites as well as the particle size, the interparticle interaction and surface chemistry [36,37]. T_C values calculated from the modified Bloch's fitting were of 621, 633, and 656 K, for NiZn1, NiZn2, and NiZn3, respectively. The noticeable difference between the values are due to the contribution of the above-mentioned intrinsic parameters. However, one can notice a monotonous decrease in T_C from NiZn1 to NiZn3. This tendency could be explained by the predominant influence of the chemical composition, in particular, the influence of the relative content of the nonmagnetic Zn^{2+} (the molar ratio Zn^{2+}/metal cations is 0.18, 0.14, and 0.11 in NiZn1, NiZn2, and NiZn3, respectively). Indeed, in spinel ferrites, T_C depends strongly on the strength of the super-exchange interaction between paramagnetic cations located in A and B sites; a high T_C traduces a strong coupling and vice versa [38]. Therefore, an increase of the fraction of the non-magnetic Zn^{2+} cation should induce a certain magnetic dilution and consequently a decrease in the strength of the super-exchange interaction. Additionally, as can be noticed from Fig. 7, the magnetization decay with temperature is low which is crucial for many applications. A measure of the decay is the temperature, $T_{1/2}$, at which the magnetization is reduced to 50%. For all three ferrites, the calculated $T_{1/2}$ values are above 372 K (~100°C) which far exceeds the ambient temperature. This allows the magnetic materials to be integrated even in industrial systems working under severe thermal environments while maintaining good magnetization response to an external magnetic field. In the case of "free" ultrafine and clusters of ferro- and ferri-magnetic particles, some theoretical calculations have shown that the Bloch's exponent, β is higher than that of the bulk counterparts (β = 3/2) and may reach 2, as a consequence of the reduction in the size of the particles [34]. The main idea behind the explanation of this finite-size effect is that the lack of full coordination at the surface of

the finite-size particles may lead to larger spin deviations in this region than in the central part of the particles. However, there have been also reports where nanoparticulated systems show lower Bloch exponents, close to the bulk value 3/2 [37]. These low values are justified in terms of the core-shell model and the effect of the matrix where the magnetic particles are embedded. In our case, the Bloch's exponent is close to the bulk value 3/2. As demonstrated by IR analysis, the anchoring of the H_2O, OH^-, and NO_3^- groups on the surface of the NiZn nanoparticles seems to strongly recover the coordination at the surface of the finite-size particles to approach the structure of full coordination of the bulk.

3.4. EBT adsorption study

The effect of various factors that could influence the adsorption process and efficiency such as the nanoparticle nature, the pH of solution, the initial EBT concentration, the nanoadsorbent dosage, and the contact time were investigated.

3.4.1. Effect of nanoparticle nature

To investigate the effect of adsorbent nature, 5 mL of 100 mg L^{-1} EBT solution (EBT dissolved in ultrapure water without any pH adjustment, pH 6.1) was simultaneously treated with 20 mg of each of three as-produced three NiZn ferrites under an agitation of 20 min. Fig. 8 depicted the UV-visible spectra of the treated EBT solutions (NiZni + EBT) along with the untreated one (untreated EBT). An important decrease in absorbance of EBT solution, and therefore an important EBT removal was observed with all ferrites. Additionally, it can be deduced from the UV-visible spectra, the removal % of EBT by NiZn2 and NiZn3 are very similar which is likely due to the particle size similarity. However, the NiZn1 ferrite shows higher removal efficiency which could be mainly due to its relatively smaller particle size as compared to the two other as-produced ferrites (Table 1); for a given mass of nanoadsorbent, the smaller the particle size, the larger the surface area and therefore the larger the number of the adsorption surface sites. Hereafter, we only focus on the study of the uptake of EBT by the NiZn1 nanoparticles. It should also be noted that the relatively higher removal efficiency of EBT by the last nanoparticles was also checked (UV-visible spectra not shown) with the pH of 2.0 of the maximum removal of EBT (section 3.4.2 "Effect of pH").

3.4.2. Effect of pH

The pH value of an aqueous environment plays a crucial role in the adsorption process, because the adsorbate–adsorbent interaction strongly depends on the surface charge of the adsorbent and the species of adsorbate. To study the effect of pH on adsorption of EBT, a fixed amount (20 mg) of the NiZn1 adsorbent was suspended in 10 mL of 100 mg L^{-1} EBT solution accurately adjusted to a certain pH value by adding 0.1 M HCl or/and 0.1 M NaOH. The mixture was agitated for 60 min. The effect of pH on the adsorption of EBT onto the particles in the pH range 2–10 is depicted in Fig. 9.

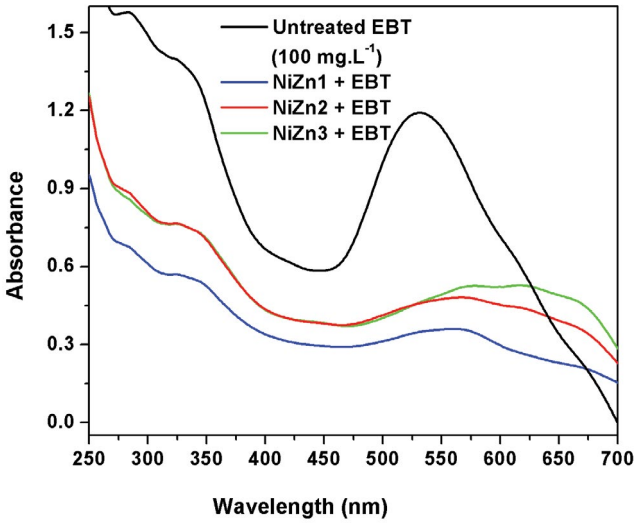

Fig. 8. Effect of the nanoparticle nature on the removal of EBT. The UV-visible spectrum of the untreated EBT solution is shown for comparison. Initial pH = 6.1, EBT volume = 5.0 mL, initial EBT concentration = 100 mg L^{-1}, nanoparticle dosage = 4.0 g L^{-1}, and contact time = 20.0 min.

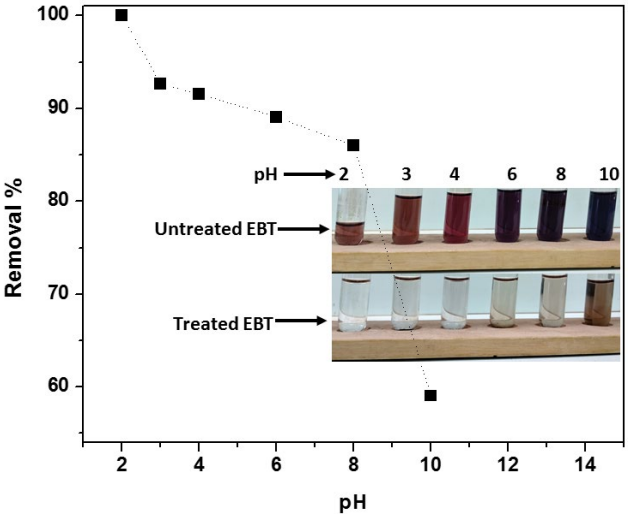

Fig. 9. Effect of the starting pH on the removal of EBT by the NiZn1 nanoparticles. The photo along with the plot shows the colour change of the untreated EBT solutions and the supernatant of the associated treated EBT ones at different pH values. EBT volume = 10.0 mL, initial EBT concentration = 100 mg L^{-1}, nanoparticle dosage = 2.0 g L^{-1}, and contact time = 60.0 min.

The EBT adsorption behavior on NiZn1 nanoparticles shows strong pH dependence and the removal capacity decreased continuously as the initial pH increased from 2 to 10 with a sharp decrease from pH 8. The uptake of the dye was of 100% and 59% at pH 2 and 10, respectively. The photo in the insert comparing the color of untreated EBT solutions and the supernatant of the treated EBT ones with the NiZn1 nanoparticles at different pH values supports the last results. EBT is an anionic dye due to its sulfonate groups

($-SO_3^-$) that are negatively charged in aqueous solutions. Whereas, as demonstrated before, for pH values below the pHpzc of ~7, the ferrite nanoparticles are positively charged at their surface with a progressively dominant ($\equiv Fe-OH_2^+$) entities as the pH decreased in the acidic range which enhances EBT adsorption through electrostatic attraction.

Further, for pH values below 7, the two hydroxyl groups of EBT are deprotonated (or at least (pKa_1 = ~6.3) one of them is protonated). These OH groups could participate to the ferrite surface through hydrogen bonding as well as electrostatic interaction through the partially charged hydroxyl groups [23]. Similarly, Attallah et al. [22] reported that the maximum adsorption of EBT dye onto the ferrite-based material, magnetite/pectin, and magnetite/silica/pectin hybrid nanocomposites was at pH about 2.0 and 3.0, respectively. Aziz et al. [16] and Sriram et al. [18] also observed a maximum adsorption efficiency of EBT onto amine activated diatom xerogels and the vegetable *Persea americana* wastes, respectively, at around pH 2.0. For pH values beyond ~7, both the EBT dye and the nanoparticles surface become negatively charged with a progressively dominant ($\equiv Fe-O^-$) entities as the pH increased from 7 to 10. This results in an increase of mutual electrostatic repulsion between the adsorbate species and adsorbent surface and therefore to a large reduction in dye adsorption onto the nanoparticles. It is worth noting that the sharp of removal % decrease beyond ~8 revealed strong electrostatic repulsion between the negatively charged surface nanoparticles and the highly dense negatively charged EBT dye (SO_3^- and two OH^-). As evident from studying the effect of pH, removal of EBT was more proficient in pH = ~2.0. Therefore, the rest of the adsorption study will be carried out at this pH value.

3.4.3. Effect of nanoparticle dosage

To investigate the effect of adsorbent dosage, 5 mL of 100 mg L^{-1} EBT solution was treated by varying dosages of adsorbent (1.0, 2, 4.0, and 6.0 g L^{-1}) for a contact time of 3.0 min at a constant starting pH 2.0 (Fig. 10). An extraordinary decrease in absorbance of EBT supernatant was observed after only 3.0 min indicating an important and a very fast decrease of EBT concentration with the increase in the number of nanoparticles. Typical photos of the EBT supernatants in comparison with the untreated 100 mg L^{-1} solution for the dosages 1.0 and 6.0 g L^{-1} are also provided as a guide for the eye.

To get a quantitative analysis of the efficiency of EBT removal, the removal % of EBT by the produced nanoparticles as well as their uptake capacity at a contact time of 3.0 min are calculated according to the equations (Eqs. (1) and (2)) and the results are plotted in Fig. 11.

From Fig. 11, it is observed that for the short contact time of 3.0 min, the removal percentage of the EBT on treating with NiZn1 nanoparticles, increased constantly up to a dosage of 6.0 g L^{-1}. For example, the removal percentage is of ~35% and 92% for the dosages of ferrite of 1.0 and 6.0 g L^{-1}, respectively. The expected result can be explained as follows: For a given number of adsorbate species, the increase in the removal percentage can be explained by the fact that the increase of sorbent dosage induced an

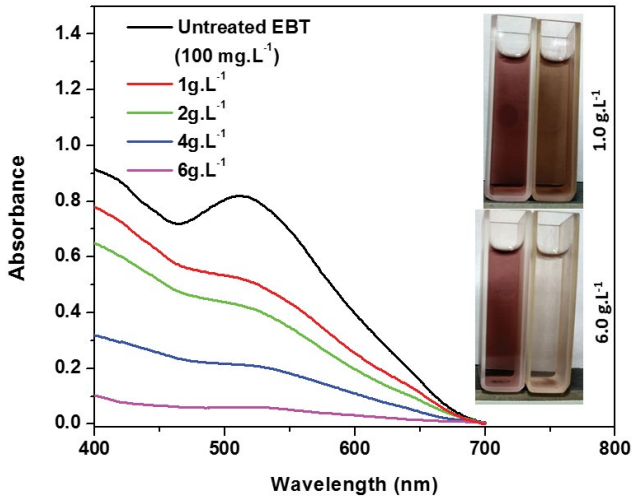

Fig. 10. Absorption spectra EBT solutions treated by different dosages of the NiZn1 nanoparticles. The inset depicts selected photos of the treated solution (in the right) in comparison with the untreated one (in the left). Initial pH = 2.0, EBT volume = 5.0 mL, initial EBT concentration = 100 mg L^{-1}, and contact time = 3.0 min.

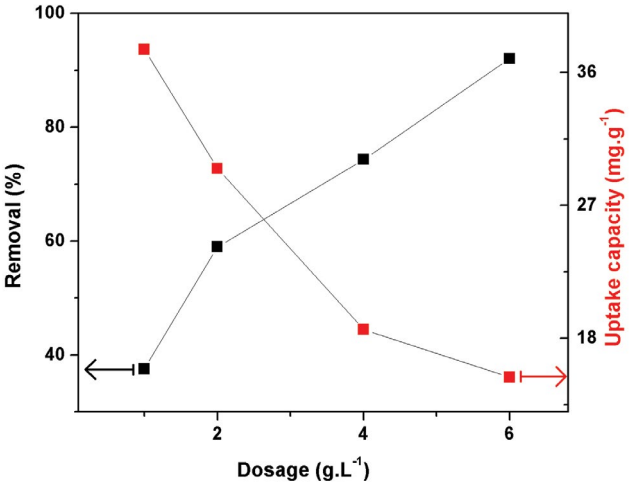

Fig. 11. Effect of the nanoparticle dosage on the EBT removal percentage and on the uptake capacity of the produced NiZn1 nanoparticles. Initial pH = 2.0, EBT volume = 5.0 mL, initial EBT concentration = 100 mg L^{-1}, and contact time = 3.0 min.

increase of the number of particles which leads to an overall surface area increase and therefore to larger number of surface adsorption sites resulting in larger number of adsorbed EBT species. For the uptake capacity, however, a monotonous decrease with the increase of the adsorbent dose can be noted. For the short contact time of 3.0 min, the uptake capacity ranges from ~38 mg g^{-1} for the dosage of 1.0 g L^{-1} to ~15 mg g^{-1} for the dosage of 6.0 g L^{-1}. For a fixed amount of adsorbate, the decrease in uptake capacity with the increase of dosage is mainly due to the presence of more surface area and therefore more adsorbent sites. Aggregation between nanoparticles due to magnetic

interaction and to high surface to volume ratio which is expected to be enhanced with the increase in nanoparticle dosage, may also contribute to the reduction of uptake capacity. Similar trend in the uptake capacity change with the adsorbent dosage, have also been observed for the removal of EBT by the 50 nm sized $NiFe_2O_4$ ferrite where the q was reported to vary between ~32 and 1.5 mg g^{-1} in the dosage range 0.25–5 g L^{-1} [19].

3.4.4. Effect of the EBT concentration and the contact time

The adsorption kinetics of the EBT uptake efficiency by the NiZn1 nanoparticles was analyzed at ambient temperature at the optimum pH (pH 2.0) in the presence of 4.0 g L^{-1} adsorbent by varying the contact time from 5 to 100 min for various initial EBT concentrations (25–250 mg L^{-1}). The plots of q_t vs. the contact time, t, for different initial EBT concentrations are presented in Fig. 12.

Form Fig. 12, it is seen that the rate of EBT uptake takes place in two stages. An initial step involving a very fast uptake of the dye species, followed by a much slower removal rate which gradually reach an equilibrium state. Moreover, whatever the concentration, more than 90% of the removable dye takes place in the first 20 min. The fast adsorption of EBT by the adsorbent could be ascribed to the external surface adsorption process of the NiZn1 nanoparticles, which is different from the microporous adsorption process. Since a large fraction of the adsorption sites of the nanoparticles exists in the exterior of the adsorbent compared with the porous adsorbent, it is easy for the adsorbate to access these active sites, thus resulting in rapid attainment of the equilibrium. Besides, the equilibrium time is a concentration–dependent parameter. It is short for the low EBT concentrations and become larger and larger with the increase of the EBT concentration. This is expected since, for a fixed adsorbent dosage, the total of available adsorption sites is also fixed and limited, while for a fixed volume of the EBT solution, the number of dye molecules become larger and larger with the increase of dye concentration. This results in a decrease in the removal percentage of the adsorbate. While, at equilibrium time, the removal efficiency of EBT was found to increase to some extent with the dye concentration. It ranges between 12.5 and ~35 mg g^{-1} for the concentrations between 50 and 250 mg L^{-1}.

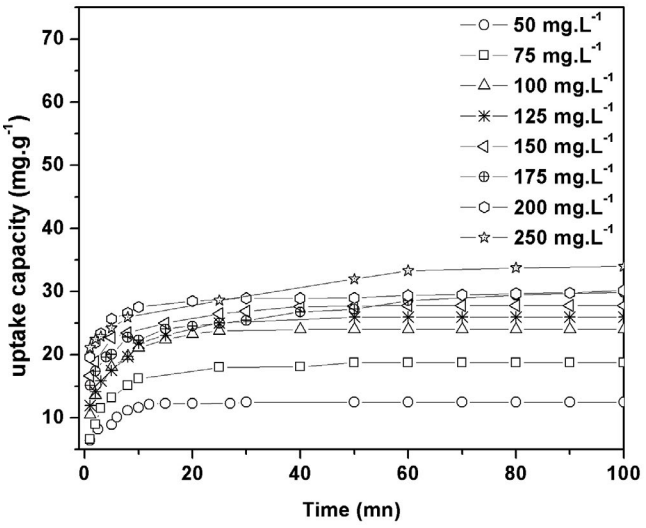

Fig. 12. EBT uptake capacity by 4.0 g L^{-1} nanoparticles dosage as a function of the contact time for different initial dye concentrations.

Three common adsorption kinetics models including the intraparticle diffusion model, the pseudo-first-order model, and the pseudo-second-order models were tested in order to define the most probable mechanism that describes the adsorption of EBT dye onto the NiZn1 nanoparticles. The integrated forms of the three models are respectively expressed as [39]:

$$q_t = k_1 \times t^{1/2} + C \tag{5}$$

$$\ln(q_e - q_t) = \ln(q_e) - k_2 \times t \tag{6}$$

$$\frac{t}{q_t} = \frac{1}{k_3 \times q_e^2} + \frac{t}{q_e} \tag{7}$$

where q_t (mg g^{-1}) is the adsorption capacity as defined by Eq. (2), q_e (mg g^{-1}) is the adsorption capacity at equilibrium time, k_1 (mg g^{-1} $min^{-1/2}$) is the intra-particle diffusion rate constant, and C is the intercept. k_2 (min^{-1}) is the rate constant for the pseudo-first-order adsorption process and k_3 (g mg^{-1} min^{-1}) is the rate constant for the pseudo-second-order adsorption. Plots of the experimental data, according to their linear forms of the variable t of the above-mentioned models are shown in Fig. 13.

It can be deduced, that the experimental data plots (Figs. 13a and b) according to Eqs. (5) and (6) associated to the intra-particle diffusion model and the pseudo-first-order model, clearly deviate from the linearity. While, whatever the EBT concentration, the experimental data points plotted (Fig. 13c) according to the linear form of Eq. (7) associated to the pseudo-second-order show excellent linearity with a correlation coefficient better than 0.986. Parameters of the pseudo-second-order model for EBT adsorption onto the NiZn nanoferrite for selected

Table 2
Parameters calculated from the best fit of the experimental data points to the pseudo-second-order for EBT adsorption onto a 4.0 g L^{-1} NiZn1 dosage for selected initial dye concentrations

EBT concentration (mg L^{-1})	50	100	150	200	250
R^2	0.999	0.998	0.981	0.989	0.986
Removal (%)	100	95.3	83	68.4	55.6
q_{eexp} (mg g^{-1})	12.5	23.8	31.4	29.9	34.8
$q_{etheo.}$ (mg g^{-1})	12.5	24.4	28.2	29.5	34.4
$C_{etheo.}$ (mg L^{-1})	0	2.3	37.0	82.2	112.3
k_3 (mg g^{-1} min^{-1}) × 10^2	7.9	3.1	2.8	4.9	1.4

Removal (%) and the q_{eexp} (mg g^{-1}) were inferred form the experimental results of Fig. 12.

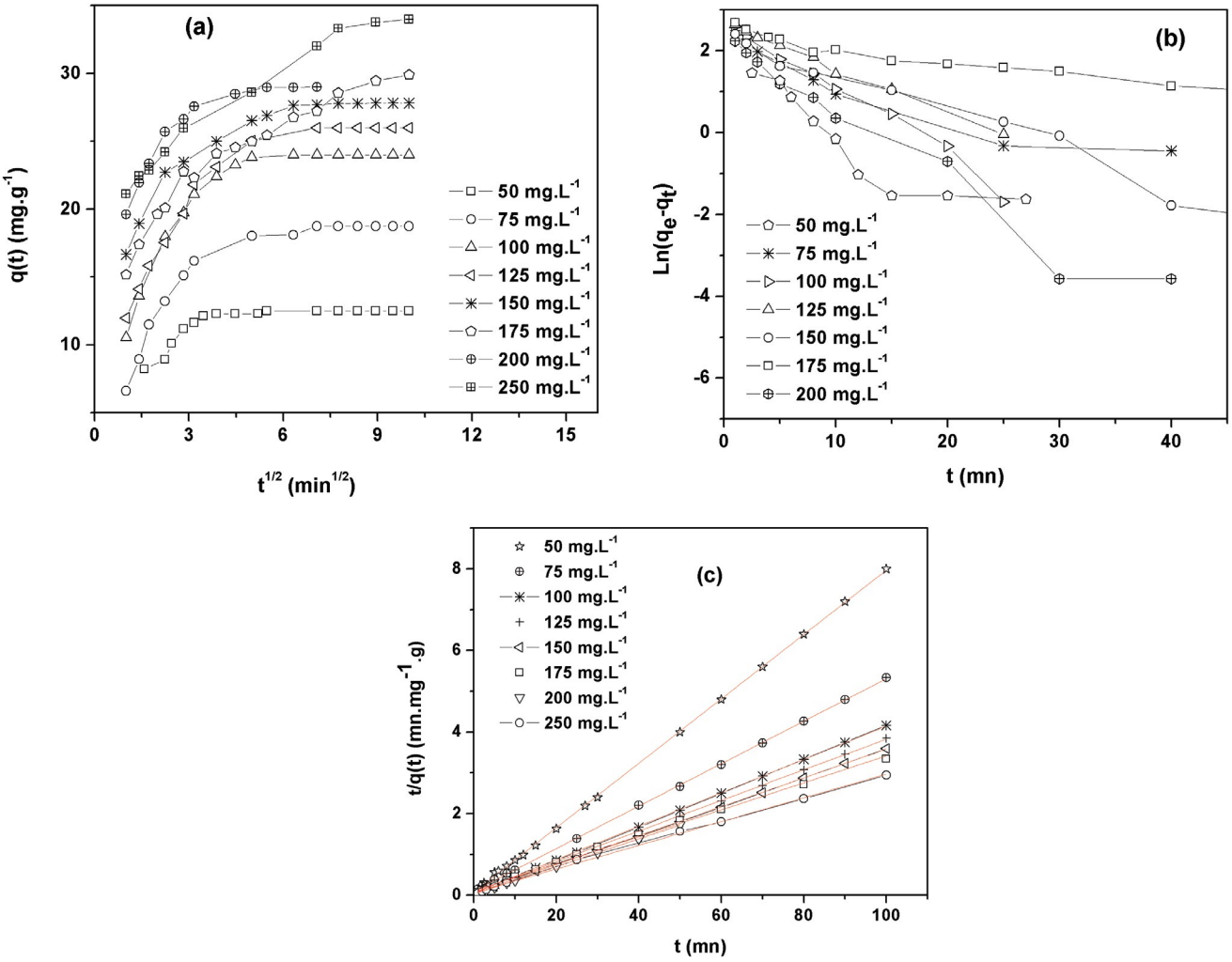

Fig. 13. Plots of the experimental data points at different initial dye concentrations, according to the equations associated to the (a) intra-particle diffusion model, the (b) pseudo-first-order model, and (c) the pseudo-second-order model of the sorption of EBT onto a 4.0 g L^{-1} NiZn1 ferrite dosage. For the plot (c), the red lines represent the best linear fit of the experimental data points to the pseudo-second-order model.

EBT initial concentrations are summarized in Table 2. The kinetics study indicated that the pseudo-second-order sorption mechanism is predominant for the sorption of the EBT entities onto our NiZn1 nanoparticles. For this model, it is considered that the rate of the sorption process is controlled by the chemisorption process. The mechanism involves valance forces through the sharing or exchange of electrons between sorbent and sorbate as covalent forces [40].

From Table 2, it can be noted that, at equilibrium, the adsorption capacity, q_e, increases with the increase of the adsorbate concentration. For instance, for the 4.0 g L^{-1} EBT dosage, the theoretical adsorption capacity, $q_{e\text{theo}}$, ranges from 12.5 for 50 to 34.4 mg g^{-1} for 250 mg g^{-1}. This can be explained by the fact that more targets of EBT provide the higher driving force to facilitate the ion diffusion from the solution to the positively charged NPs surfaces, and therefore more collisions between EBT ions and active sites of the sorbent. Besides, it is important to notice that as outlined before (section 3.4.3 "Effect of nanoparticle dosage"), the adsorption capacity, q_e, is expected to be higher for low adsorbate dosages.

3.4.5. Regeneration and reuse of the nanoparticles

As demonstrated before (section 3.4.2 "Effect of pH"), adsorption of EBT dye on NiZn1 nanoparticles surface decreases drastically with the pH increase. Therefore, desorption of the dyes and therefore regeneration of the adsorbent could be performed at high alkaline pH values. Adsorption–desorption–regeneration tests were conducted on a 50 mL EBT solution with an initial concentration of 50 mg L^{-1} and a nanoparticles dose of 1.0 g L^{-1}. To test the reusability of the nanoadsorbent, the following detailed procedure was adopted: In a first step, the nanoparticles were shacked with the EBT solution for 10 min. Then, the absorbance of the supernatant was measured after decantation with the aid of NdFeB magnet. After that, to remove the

adsorbed EBT species, the EBT–loaded nanoparticles were dispersed in an excess (about 25 mL) of 0.5 M NaOH and then the mixture was shacked for about 5.0 min. Clearly, the recuperated supernatant shows the characteristic color of water soluble EBT. The last step was repeated and a complete desorption of EBT (complete decolorization of the supernatant) was reached as confirmed by UV-visible. The adsorbent was then thoroughly washed with ultrapure deionizer water till the pH of the wash water become neutral and finally washed with ethanol and dried at 60°C for about 1 h. The regenerated nanoparticles were subjected to subsequent runs under the same conditions as described before. Six consecutive adsorption–desorption–regeneration cycles were carried out to validate the reusability of the produced nanoparticles. Fig. 14 shows the removal efficiency of EBT during the six cycles of adsorption–desorption–regeneration. As can be seen, a good reproducibility of the adsorption capacity of the nanoadsorbent during the number of cycles was achieved, which indicated that there were no noticeable nanoparticles loss and/or irreversible adsorbent sites on the surface of the adsorbent. Additionally, one can notice the high chemical stability of the produced nanoparticles in a relatively strongly acidified medium (pH 2.0). These advantages along with the ultrafine microstructure and the reasonable magnetization and high Curie temperature make our nanoferrite a promising candidate for wastewater treatments even in severe conditions.

It is interesting to compare the physical characteristics and the adsorption–desorption performance of our as-synthesized nanoparticles with other adsorbents towards the EBT dye (Table 3). Referring to Table 3, one can notice that (i) for the magnetic nanoparticles-based adsorbents (the first four adsorbents), we expect that our nanoparticles should have the easiest, the most scalable, and the

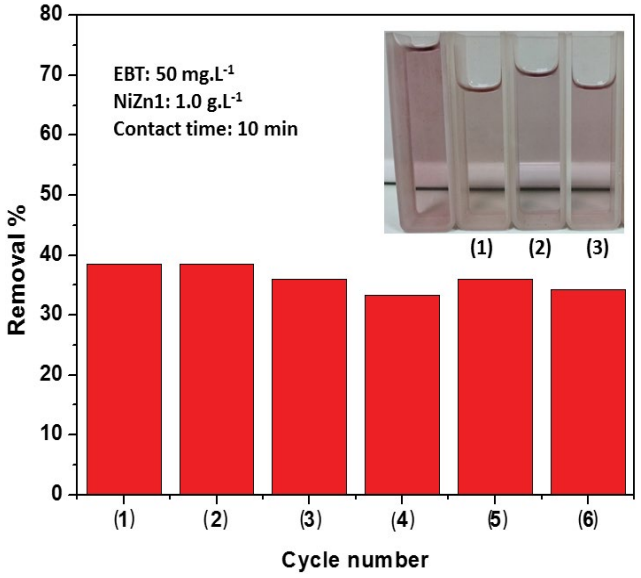

Fig. 14. Reusability of the NiZn1 nanoadsorbent for the adsorption–desorption of EBT dye during six cycles. The inset is a photo comparing the untreated EBT solution (left) to the supernatants (right) of the first three EBT adsorption–desorption–regeneration cycles.

Table 3
Comparison of selected microstructural and magnetic characteristics, and adsorption–desorption performance of our as-prepared NiZn1 nanoferrite with other selected magnetic and non-magnetic adsorbents for the removal of the EBT dye

Adsorbent	Elaboration method	Particle size	[a]M_{sat} (emu g^{-1})	Optimum pH	Adsorption capacity (mg g^{-1})	Reusability performance (%); number of cycles	Reference
NiZn1	Modified classical coprecipitation	~14 nm	~56	~2	~30	~89; 6 cycles	The present study
$Fe_{3O}4$	Coprecipitation in triethyl amine	~20–40 nm	~29	~4–5	~89	~86; 3 cycles	[23]
$NiFe_2O_4$	Reverse coprecipitation	~50 nm	Unknown	~6	~32	Not done	[19]
Magnetite/silica/pectin hybrid	Coprecipitation/hydrolysis/condensation	~6 nm	~30	~2	~65	~25; 3 cycles	[22]
Activated carbon	*Persea americana nuts* carbonization	Unknown	NA	~2	~120	~55; 5 cycles	[16]
Diatomaceous earth	Hydrothermal	Micro particles	NA	~2	~14	Not done	[17]
Diatom-silica xerogel-ceria	Sol–gel	Micro particles	NA	~2	~47	~67; 5 cycles	[17]
Amine activated diatom xerogel	Several steps (Scheme 1 of [18])	Micro particles	NA	~2	~62	~83; 5 cycles	[18]
Waste activated sludge	HCl-acidified waste sludge	Unknown	NA	~6	~14	Not done	[11]
MnO_2-coated Zeolite	$KMnO_4$/HCl-treated zeolite	Unknown	NA	Unknown	~4	Not done	[20]
H_3PO_4-modified berry leaves	Chemical impregnation/carbonization	Unknown	NA	~7	~133	~88; 3 cycles	[21]
Activated carbon	Waste rice hulls carbonization	300–500 µm	NA	~2	~2	Not done	[41]

[a]NA, not applicable.

cheapest chemical procedure. (ii) Our nanoparticles exhibited the largest saturation magnetization, which is a curtail intrinsic parameter for the ease and quick magnetic separation of the adsorbent from the supernatant. (iii) The adsorption capacity, q_e, of our NiZn1 nanoferrite is reasonable compared to the other nanoadsorbents, and as outlined before, this capacity is expected to be much larger for low adsorbent dosages. (iv) Our nanoparticles are highly regenerable, with a performance after successive six runs of about 90%. (v) A fast removal rate was observed for our nanoparticles, and more than 90% of the removable adsorbents were achieved in less than 20 min and the equilibrium state for the EBT removal is reached in less than 100 min, even for EBT concentration as high as 250 mg L^{-1}.

4. Conclusion

The phase purity, the structure, the microstructure, the surface functionality, and the magnetic properties of a series of NiZn nanoferrites were investigated by various characterization techniques. EDX, XRD, and IR analyses showed that the as-produced powders are pure ultrasmall nanoparticles with ~13–16 nm size. The nanoferrites exhibited a room-temperature superparamagnetic behavior with reasonable saturation magnetization (M_{sat} ranges from 56 to 65 emu g^{-1}) and high Curie temperature (T_C ranges from 621 to 656 K). The large T_C (along with their good chemical stability) confer to the produced nanoparticles the advantage for their utilization in severe conditions of environmental/industrial wastewater treatments. The room-temperature adsorption of the EBT dye onto the produced nanocrystals was found to be dependent on the nanoparticle nature and the best adsorption capacity was found with the smaller nanoparticles (NiZn1). Additionally, it was shown that the removal efficiency was very rapid and depends strongly on the pH; the lower the pH, the larger the adsorption capacity. At the optimum pH (pH 2.0), the uptake capacity was found to decrease with the increase in nanoparticle dosage. For instance, for the contact time of 3.0 min, the uptake capacity was found to range from ~38 mg g^{-1} for the dosage of 1.0 g L^{-1} to ~15 mg g^{-1} for the dosage of 6.0 g L^{-1}. The kinetic study revealed that the pseudo-second-order model fitted well the experimental data ($R^2 > 0.986$). The adsorption capacity, q_e, of NiZn1 was found to increase with the increase of the adsorbate concentration. For instance, for a 4.0 g L^{-1} EBT dosage, q_e was found to range from 12.5 for 50 mg g^{-1} to 34.4 for 250 mg g^{-1}. Furthermore, for a technological application point of view, the NiZn1 nanoadsorbent was tested in six adsorption–desorption cycles without noticeable decrease in its performance. An in-depth research work aiming further improvement of the uptake and the recycling efficiency of the produced nanoparticles by functionalizing their surface with various affordable bifunctional ligands is currently under process.

Acknowledgment

The authors are greatly indebted to the deanship of Scientific Research at Northern Border University for its funding of the present research work through the research project No. SCI-2018-3-9-F-7732.

References

[1] J. Smit, H.P.J. Wijn, Ferrites, Philips Technical Library, Eindhoven, The Netherlands, 1959.
[2] B. Pacakova, S. Kubickova, A. Reznickova, D. Niznansky, J. Vejpravova, Spinel Ferrite Nanoparticles: Correlation of Structure and Magnetism, Magnetic Spinels - Synthesis, Properties and Applications, IntechOpen, 2017. Available at: https://www.intechopen.com/books/magnetic-spinels-synthesis-properties-and-applications/spinel-ferrite-nanoparticles-correlation-of-structure-and-magnetism (accessed 21 October 2019).
[3] M.A. Iqbel, M.U. Islam, I. Ali, M.A. Khan, I. Sadiq, I. Ali, High frequency dielectric properties of Eu^{+3}-substituted Li–Mg ferrites synthesized by sol–gel auto-combustion method, J. Alloys Compd., 586 (2014) 404–410.
[4] A.S. Teja, P.Y. Koh, Synthesis, properties, and applications of magnetic iron oxide nanoparticles, Prog. Cryst. Growth Charact. Mater., 55 (2009) 22–45.
[5] C.N.R. Rao, H.C. Mult, A. Müller, A.K. Cheetham, The Chemistry of Nanomaterials: Synthesis, Properties and Applications, Wiley-VCH, Weinheim, Germany, 2004.
[6] A.K. Haghi, A.K. Zachariah, N. Kalarikkal, Nanomaterials Synthesis, Characterization, and Applications, S. Thomas, M. Sebastien, A. George, Y. Weimin, Eds., Advances in Nanoscience and Nanotechnology, Vol. 3, Apple Academic Press, New Jersey, USA, 2013.
[7] A. Roy, J. Bhattacharya, Nanotechnology in Industrial Wastewater Treatment, IWA Publishing, London, 2015.
[8] S. Kanagesan, M. Hashim, A.B. Aziz, I. Ismail, S. Tamilselvan, N.B. Alitheen, M.K. Swamy, B.P.C. Rao, Evaluation of antioxidant and cytotoxicity activities of copper ferrite ($CuFe_2O_4$) and zinc ferrite ($ZnFe_2O_4$) nanoparticles synthesized by sol-gel self-combustion method, Appl. Sci., 6 (2016) 184–196.
[9] B.I. Kharisov, H.V.R. Dias, O.V. Kharissova, Mini-review: ferrite nanoparticles in the catalysis, Arabian J. Chem., 12 (2019) 1234–1246.
[10] A.M. Gutierrez, T.D. Dziubla, J.Z. Hilt, Recent advances on iron oxide magnetic nanoparticles as sorbents of organic pollutants in water and wastewater treatment, Rev. Environ. Health, 32 (2017) 111–117.
[11] M.A.A. Eldeen, A.A.M.E. Sayed, D.M.S.A. Salem, G.M.E. Zokm, The uptake of Eriochrome Black T dye from aqueous solutions utilizing waste activated sludge: adsorption process optimization using factorial design, Egypt. J. of Aquat. Res., 44 (2018) 179–186.
[12] K.R. Kunduru, M. Nazarkovsky, S. Farah, R.P. Pawar, A. Basu, S. Pawar, A.J. Domb, Nanotechnology for Water Purification: Applications of Nanotechnology Methods in Wastewater Treatment, M.G. Alexandru, Ed., Water Purification Nanotechnology in the Agri-Food Industry, Academic Press, Cambridge, 2017, pp. 33–74.
[13] P. Sukanchan, Application of Nanotechnology in Water Treatment, Wastewater Treatment and Other Domains of Environmental Engineering Science–A Broad Scientific Perspective and Critical Review, A.K. Mishra, C.M. Hussain, Eds., Nanotechnology for Sustainable Water Resources, Scrivener Publishing LLC, Beverly, USA, 2018, pp. 1–39.
[14] A. Figoli, M.S.S. Dorraji, A.R.A. Ghadim, Application of Nanotechnology in Drinking Water Purification, M.G. Alexandru, Ed., Water Purification, Academic Press, New Jersey, USA, 2017, pp. 119–167.
[15] D.H.K. Reddy, Y.S. Yun, Spinel ferrite magnetic adsorbents: alternative future materials for water purification, Coord. Chem. Rev., 315 (2016) 90–111.
[16] E.K. Aziz, R. Abdelmajid, L.M. Rachid, E.H. Mohammadine, Adsorptive removal of anionic dye from aqueous solutions using powdered and calcined vegetables wastes as low-cost adsorbent, Arabian J. Basic Appl. Sci., 25 (2018) 93–102.
[17] G. Sriram, U.T. Uthapp, R.M. Rego, M. Kigga, T. Kumeria, H.Y. Jung, M.D. Kurkuri, Ceria decorated porous diatom-xerogel as an effective adsorbent for the efficient removal of Eriochrome Black T, Chemosphere, 238 (2020) 124692.

[18] G. Sriram, M.P. Bhat, M. Kigga, U.T. Uthappa, H.Y. Jung, T. Kumeria, M.D. Kurkuri, Amine activated diatom xerogel hybrid material for efficient removal of hazardous dye, Mater. Chem. Phys., 235 (2019) 121738.
[19] M. Farid, A. Asma, K. Maryam, Efficient removal of Eriochrome Black T from aqueous solution using $NiFe_2O_4$ magnetic nanoparticles, J. Environ. Health Sci. Eng., 12 (2014) 1–7.
[20] D.M.M. Aguila, M.V. Ligaray, Adsorption of Eriochrome Black T on MnO_2-coated zeolite, Int. J. Environ. Sci. Dev., 6 (2015) 824–827.
[21] M. Ahmaruzzamana, M.J.K. Ahmed, S. Begum, Remediation of Eriochrome Black T-contaminated aqueous solutions utilizing H_3PO_4-modified berry leaves as a non-conventional adsorbent, Desal. Water Treat., 56 (2015) 1–13.
[22] O.A. Attallah, M.A. Al-Ghobashy, M. Nebsen, M.Y. Salem, Removal of cationic and anionic dyes from aqueous solution with magnetite/pectin and magnetite/silica/pectin hybrid nanocomposites: kinetic, isotherm and mechanism analysis, RSC Adv., 6 (2016) 11461–11480.
[23] B. Saha, S. Das, J. Saikia, G. Das, Preferential and enhanced adsorption of different dyes on iron oxide nanoparticles: a comparative study, J. Phys. Chem. C, 115 (2011) 8024–8033.
[24] L.B. Tahar, M.H. Oueslati, M.J.A. Abualreish. Synthesis of magnetite derivatives nanoparticles and their application for the removal of chromium(VI) from aqueous solutions, J. Colloid Interface Sci., 512 (2018) 115–126.
[25] D. Zins, V. Cabuil, R. Massart, New aqueous magnetic fluids, J. Mol. Liq., 83 (1999) 217–232.
[26] X'Pert HighScore Plus V2, PANAlytical, P.V, Almelo, The Netherlands, 2003.
[27] J.I. Langford, A.J.C. Wilson, Scherrer after sixty years: a survey and some new results in the determination of crystallite size, J. Appl. Crystallogr., 11 (1978) 102–113.
[28] S.A. Albuquerque, J.D. Ardisson, W.A.A. Macedo, Nanosized powders of NiZn ferrite: synthesis, structure, and magnetism, J. Appl. Phys., 87 (2000) 4352–4357.
[29] H. Huili, B. Grindi, G. Viau, L.B. Tahar, Effect of cobalt substitution on the structure, electrical, and magnetic properties of nanorcrystalline $Ni_{0.5}Zn_{0.5}Fe_2O_4$ prepared by the polyol process, Ceram. Int., 40 (2014) 16235–16244.
[30] R. Kato, J. Rolfe, Vibration frequencies of NO_2^- and NO_3^- ions in KBr crystals, J. Chem. Phys., 47 (1967) 901–1910.
[31] R.M. Cornell, U. Schwertmann, The Iron Oxides, 2nd ed., VCH, Weimheim, 2003.
[32] M. Kosmulski, pH-dependent surface charging and points of zero charge II. Update, J Colloid Interface Sci., 275 (2004) 214–224.
[33] M.P. Pileni, Magnetic fluids: fabrication, magnetic properties, and organization of nanocrystals, *Adv. Funct*. Mater., *11 (*2001) *323–336*.
[34] A. Demortière, P. Panissod, B.P. Pichon, G. Pourroy, D. Guillon, B. Donnio, S.B. Colin, Size-dependent properties of magnetic iron oxide nanocrystals, Nanoscale, 3 (2011) 225–232.
[35] M. Artus, L.B. Tahar, F. Herbst, L. Smiri, F. Villain, N. Yaacoub, J.M. Grenèche, S. Ammar, F. Fiévet, Size-dependent magnetic properties of $CoFe_2O_4$ nanoparticles prepared in polyol, J. Phys. Condens. Matter, 23 (2011) 506001 (9pp).
[36] J.Z. Zhang, Z.L. Wang, B.C. Chakoumakos, J.S. Yin, Temperature dependence of cation distribution and oxidation state in magnetic Mn-Fe ferrite nanocrystals, J. Am. Chem. Soc., 120 (1998) 1800–1804.
[37] D. Ortega, E.V. Fort, D.A. Garcia, R. Garcia, R. Litrán, C. Barrera-Solano, M.R. del-Solar, M. Domínguez, Size and surface effects in the magnetic properties of maghemite and magnetite coated nanoparticles, Philos. Trans. R. Soc. London, Ser. A, 368 (2010) 4407–4418.
[38] M.A. Gilleo, Superexchange interaction in ferrimagnetic garnets and spinels which contain randomly incomplete linkages, J. Phys.Chem. Solids, 13 (1960) 33–39.
[39] R. Gong, J. Ye, W. Dai, X. Yan, J. Hu, X. Hu, S. Li, H. Huang, Adsorptive removal of methyl orange and methylene blue from aqueous solution with finger-citron-residue-based activated carbon, Ind. Eng. Chem. Res., 52 (2013) 14297–14303.
[40] Y.S. Ho, G. McKay, Pseudo-second order model for sorption processes, Process Biochem, 34 (1999) 451–465.
[41] M.D.G. De Luna, E.D. Flores, D.A.D. Genuino, C.M. Futalan, M.W. Wan, Adsorption of Eriochrome Black T (EBT) dye using activated carbon prepared from waste rice hulls-optimization, isotherm and kinetic studies, J. Taiwan Inst. Chem. Eng., 44 (2013) 646–653.